Does the normal stress parallel to the sliding plane affect the friction of ice upon ice?

Andrew L. FORTT, Erland M. SCHULSON

Ice Research Laboratory, Thayer School of Engineering, Dartmouth College, Hanover, New Hampshire 03755-8000, USA
E-mail: andrew.l.fortt@dartmouth.edu

ABSTRACT. Sliding experiments were performed at –10°C on smooth surfaces of freshwater columnar-grained S2 ice sliding against itself at a velocity of 8×10^{-4} m s^{-1}, with the purpose of examining whether normal stress parallel to the sliding plane affects frictional resistance. This component of the stress tensor was varied (0.20–1.83 MPa) using a loading system operated under biaxial compression, by orienting the sliding plane at two different angles, 26° and 64°, with respect to the principal loading direction. Under these conditions, no evidence was found to indicate that the normal stress in the direction of sliding affects the friction coefficient.

1. INTRODUCTION

In modeling failure of the arctic sea-ice cover, Schreyer and others (2006) invoked frictional sliding by incorporating a Coulombic failure envelope. In so doing, they questioned whether, in addition to traction on the plane of material failure (i.e. in addition to the normal (σ_{nn}) and shear (σ_{nt}) components of traction; Fig. 1), the normal component of stress, σ_{tt} (Fig. 1), that is oriented parallel to the sliding plane might affect the sliding resistance. The question is not limited to the arctic sea-ice cover, but applies as well to tectonic evolution of icy bodies of the outer solar system, such as Jupiter's moon Europa (Tufts and others, 1999; Kattenhorn, 2004) and Saturn's satellite Enceladus (Nimmo and others, 2007; Smith-Konter and Pappalardo, 2008). Schreyer and others (2006) did not expand upon the underlying physics, although one could imagine that under all-compressive loading, the stress component σ_{tt} might act to prevent either formation or propagation of surface cracks inclined to both the sliding plane and sliding direction, of the kind reported by Montagnat and Schulson (2003).

To determine whether this third component of stress (where the tensor is expressed in terms of a coordinate system defined by the failure plane and by the direction of sliding) actually affects the measured resistance to sliding, a series of experiments was performed in which the two normal components of the stress tensor were varied independently. The results are reported here. To our knowledge, this is the first report to examine this point experimentally.

2. EXPERIMENTAL PROCEDURE

We chose to examine columnar-grained, polycrystalline ice that possesses the S2 (Michel and Ramseier, 1971) growth texture, and to slide the ice across itself, column against column, in a direction normal to the long axis of the grains, in the manner that a sheet of first-year sea ice might slide across a closed lead or Coulombic fault (Schulson, 2004). For simplicity, we examined freshwater ice, since there is little to distinguish the Coulombic failure envelope of the two kinds of material (Schulson and others, 2006a). We made the ice in the laboratory by unidirectionally freezing local tap-water, and then verified its microstructure, as described elsewhere (Fortt and Schulson, 2007). Subsequently, we prepared plate-shaped specimens of dimensions 160 mm × 80 mm × 50 mm, with the long axis of the columnar grains oriented perpendicular to the largest faces. To prepare a sliding interface, we cut the specimens diagonally from corner to corner, as sketched in Figure 2, and then polished the exposed faces by gently rubbing using a warm, optically flat glass plate on a lapping stone. The surface roughness in the direction of sliding was obtained using a stylus profilometer and found to be $(4 \pm 2) \times 10^{-6}$ m. To hold together the two wedge-shaped blocks (Fig. 2) during preloading, holes of 5 mm diameter were drilled along the X_3 direction and joined by a piece of string. To allow sliding without crushing the apex of each wedge, shims of chemically polished brass were placed on the top and the bottom of the wedges (Fig. 2). To reduce friction along the ice–shim interface, thin (0.15 mm) polyethylene sheets were inserted.

We oriented specimens for sliding in one of two ways. In the first, the long axis of the specimen was oriented parallel to the X_1 axis (Fig. 2a) and the sliding plane was inclined by $\theta \sim 26^\circ$ to X_1, but parallel to the direction of the columns, X_3. In the second, the long axis of the specimen was oriented parallel to X_2 (Fig. 2b) and the sliding plane was inclined by $\theta \sim 64^\circ$ to X_1. In both cases, the specimens were loaded under biaxial compression where the major stress, σ_1, was applied along direction X_1 and the minor stress, σ_2, was applied along direction X_2, using a true multiaxial loading system housed within a cold room of Dartmouth's Ice Research Laboratory. Assuming frictionless contact between the ice and loading shims, the ratio, χ, of the normal stresses parallel to the plane of sliding σ_{tt} and perpendicular to the plane of sliding σ_{nn} is given by

$$\chi \equiv \frac{\sigma_{tt}}{\sigma_{nn}} = \frac{\sigma_1 \cos^2\theta + \sigma_2 \sin^2\theta}{\sigma_1 \sin^2\theta + \sigma_2 \cos^2\theta}. \quad (1)$$

For the geometry of the two set-ups and for the values measured for the two applied stresses (given below), this parameter varied by about a factor of two, from $\chi \sim 1.4$ for $\theta \sim 26^\circ$ to $\chi \sim 0.65$ for $\theta \sim 64^\circ$.

To effect sliding, a constant displacement rate, V_A, was applied in the X_1 direction and then converted to sliding speed, V_S, along the inclined plane through the expression

$$V_S = \frac{V_A}{\cos\theta}. \quad (2)$$

For the two different orientations of the sliding plane, the

https://doi.org/10.3189/002214311798043771 Published online by Cambridge University Press

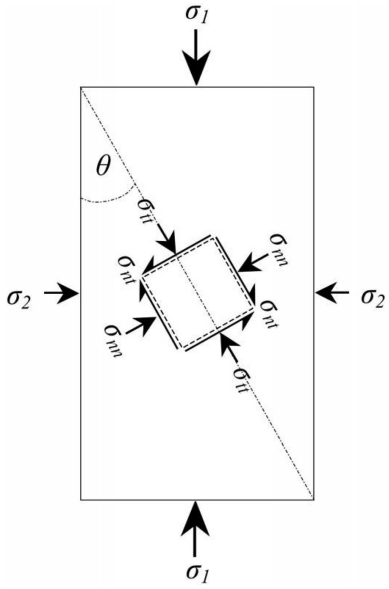

Fig. 1. Schematic diagram showing orientation of stresses with respect to sliding plane. σ_1 and σ_2 are the principal stresses with respect to the loading system, σ_{nn} is the normal stress perpendicular to the sliding plane, σ_{tt} is the normal stress parallel to the sliding plane in the direction of sliding and σ_{nt} is the shear stress on the sliding plane.

applied velocity was such that the sliding speed in both cases was $V_S = 8 \times 10^{-4}$ m s^{-1}. The velocity was chosen as it is within the range of velocities observed in the arctic ice pack (Moritz and Stern, 2001). The ice was slid a total distance of 8 mm, recorded by extensometers that were attached to the loading platens. In all tests the temperature of the ice was –10°C. During each test, the loads applied in the two directions X_1 and X_2 were recorded electronically at a rate of 1000 scans s^{-1} and then converted to the principal stresses σ_1 and σ_2. Loads were measured with a sensitivity of ±100 N, which translated to a sensitivity in principal stress of ±0.03 MPa on the smaller faces and ±0.015 MPa on the larger faces. The experiments were performed such that the minor stress, σ_2, was held constant for the duration of each test and the range of normal stresses tested was chosen to reflect that observed in the arctic ice pack (albeit on the lower side of our range).

3. RESULTS

We performed a total of 18 experiments, 11 for the orientation of the sliding plane $\theta \sim 26°$ and 7 for $\theta \sim 64°$. Figure 3 shows examples of load-displacement curves from which the appropriate stresses were computed (using the midpoint of the load at each displacement). Table 1 lists the results. Listed in the table are the computed values of the two normal stresses and the computed value of the shear stress, σ_{nt}, after sliding different amounts (0, 2.4 mm, 4 mm, 8 mm).

Figure 4 plots the shear stress on the sliding plane versus the normal stress acting across the sliding plane, after displacement, δ_S, of 0, 2.4, 4 and 8 mm, for both orientations of the sliding plane. The displacements were chosen to enable comparisons to be made with our previous work (Fortt and Schulson, 2007). The curves may be described reasonably well by straight lines (coefficient of determination R^2 shown in the figure), in keeping with earlier measurements of frictional sliding of ice sliding slowly upon itself under a relatively low normal stress (Fortt and Schulson, 2007). The coefficient of friction is given by the slope of the curves (more below) and appears to be higher ($\mu = 0.27$) and more variable at the onset of sliding than during sliding where it increases from $\mu = 0.16$ at a displacement of $\delta_S = 2.4$ mm to $\mu = 0.21$ at $\delta_S = 8$ mm. The implication is that the static coefficient of friction is greater than the kinetic coefficient. This is not surprising given the added time for sintering before the test starts. There also appears to be a systematic trend of increasing friction with increasing displacement. However, we prefer not to place too fine a point on this trend until further work is done. Of particular interest from the perspective of these experiments is the observation that within experimental uncertainty the data for the two orientations fall upon the same line for each displacement. This implies that under the present conditions the normal component of the stress tensor parallel to the

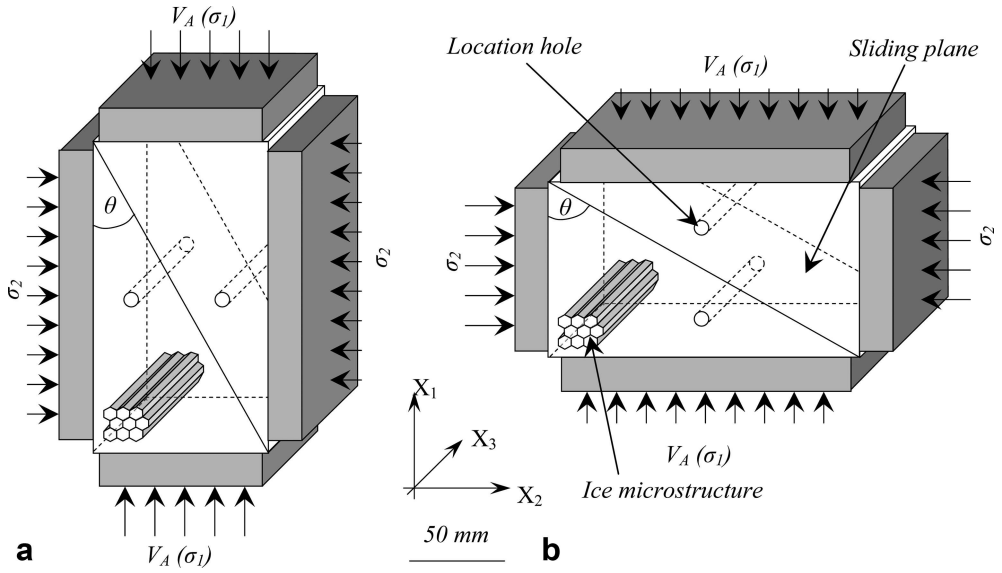

Fig. 2. Schematic diagram showing experimental set-up of (a) 26° oriented sliding plane test, and (b) 64° oriented sliding plane test.

https://doi.org/10.3189/002214311798043771 Published online by Cambridge University Press

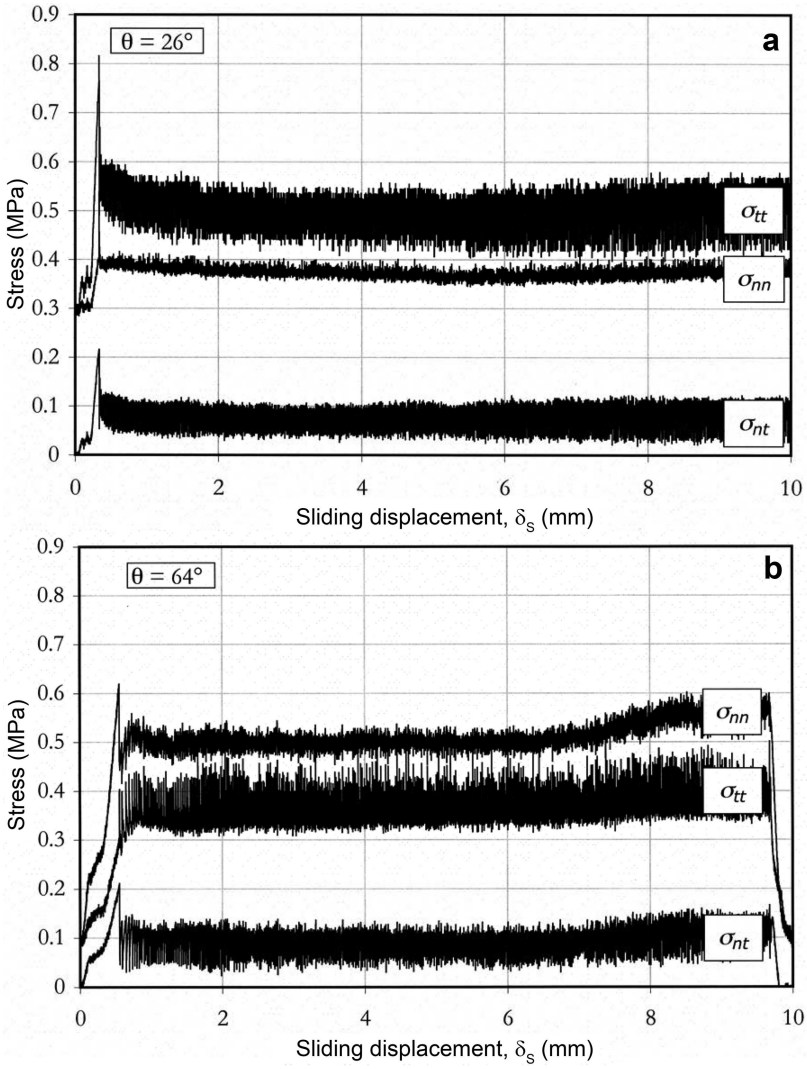

Fig. 3. Examples of stress-vs-sliding-displacement curves for (a) 26° oriented sliding plane test and (b) 64° oriented sliding plane test.

Table 1. Experimental results. Test No. indicates the Ice Research Laboratory test label, θ is the measured angle of the sliding plane with respect to X_1, δ_S is the sliding displacement, σ_{nn} is the normal stress perpendicular to the sliding plane, σ_{nt} is the shear stress on the sliding plane and σ_{tt} is the normal stress parallel to the sliding plane. Italics signify the 64° tests, whereas the 26° tests are in regular font.

		$\delta_S = 0.0$ mm			$\delta_S = 2.4$ mm			$\delta_S = 4.0$ mm			$\delta_S = 8.0$ mm		
Test No.	θ	σ_{nn}	σ_{nt}	σ_{tt}	σ_{nn}	σ_{nt}	σ_{tt}	σ_{nn}	σ_{nt}	σ_{tt}	σ_{nn}	σ_{nt}	σ_{tt}
	°	MPa	MPa	MPa	MPa	MPa	MPa	MPa	MPa	MPa	MPa	MPa	MPa
262	24	0.55	0.22	0.94	0.52	0.11	0.71	0.53	0.13	0.77	0.53	0.13	0.77
721	27	0.51	0.26	0.90	0.45	0.08	0.57	0.45	0.08	0.57	0.45	0.09	0.59
722	27	0.36	0.15	0.59	0.22	0.06	0.30	0.22	0.05	0.29	0.21	0.05	0.29
723	25	0.49	0.18	0.80	0.30	0.07	0.43	0.30	0.07	0.42	0.29	0.07	0.42
724	25	0.54	0.21	0.81	0.37	0.07	0.49	0.36	0.07	0.49	0.37	0.07	0.50
725	26	0.31	0.16	0.55	0.16	0.06	0.26	0.17	0.06	0.27	0.17	0.04	0.22
726	26	0.27	0.12	0.45	0.16	0.04	0.23	0.16	0.04	0.21	0.16	0.03	0.20
727	25	0.92	0.29	1.41	0.65	0.14	0.88	0.65	0.14	0.88	0.67	0.14	0.90
728	25	0.92	0.28	1.40	0.69	0.14	0.93	0.71	0.16	0.99	0.71	0.14	0.94
729	24	0.82	0.23	1.24	0.76	0.14	1.02	0.77	0.15	1.04	0.77	0.17	1.08
730	24	1.12	0.39	1.83	0.82	0.16	1.11	0.81	0.15	1.08	0.83	0.20	1.18
749	*65*	*0.61*	*0.18*	*0.30*	*0.53*	*0.13*	*0.32*	*0.56*	*0.14*	*0.33*	*0.61*	*0.16*	*0.35*
752	*64*	–	–	–	*0.63*	*0.11*	*0.44*	*0.66*	*0.12*	*0.47*	*0.78*	*0.16*	*0.52*
753	*64*	*0.71*	*0.22*	*0.35*	*0.69*	*0.12*	*0.51*	*0.69*	*0.11*	*0.50*	*0.82*	*0.17*	*0.55*
754	*64*	*0.62*	*0.21*	*0.29*	*0.51*	*0.09*	*0.37*	*0.51*	*0.09*	*0.37*	*0.55*	*0.10*	*0.38*
755	*64*	*0.52*	*0.13*	*0.31*	*0.50*	*0.09*	*0.36*	*0.52*	*0.10*	*0.37*	*0.57*	*0.12*	*0.38*
756	*64*	–	–	–	*0.41*	*0.08*	*0.28*	*0.42*	*0.09*	*0.28*	*0.45*	*0.10*	*0.30*
757	*64*	*0.49*	*0.16*	*0.24*	*0.56*	*0.11*	*0.40*	*0.57*	*0.11*	*0.40*	*0.61*	*0.12*	*0.42*

https://doi.org/10.3189/002214311798043771 Published online by Cambridge University Press

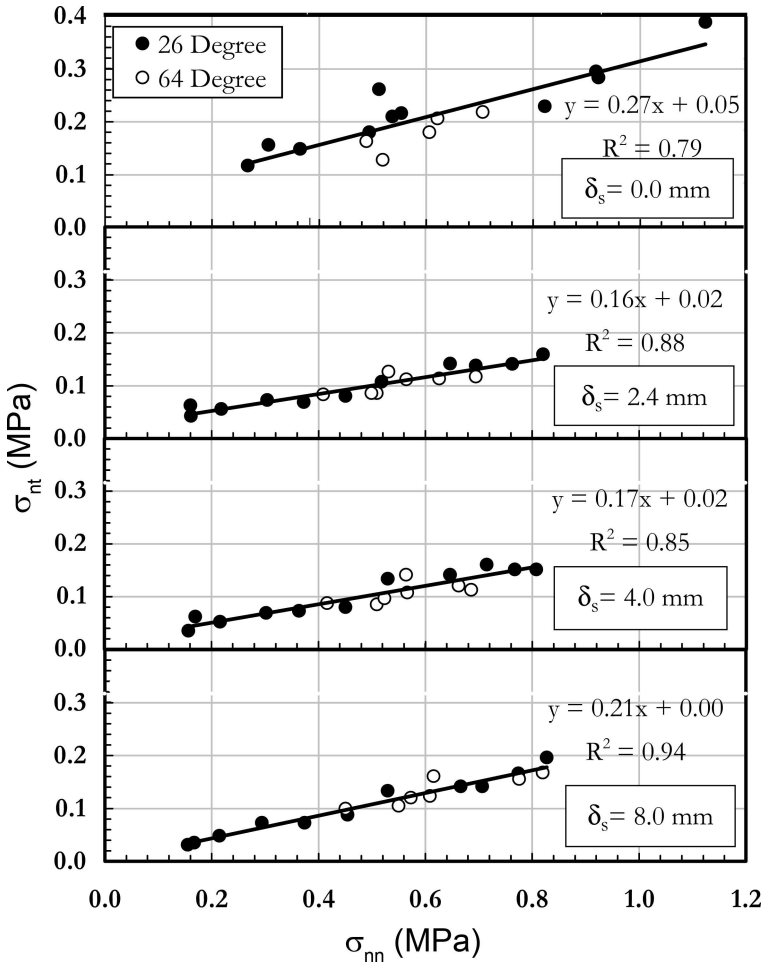

Fig. 4. Graph of σ_{nt} vs σ_{nn} at four sliding displacements. Black (solid) points indicate 26° data points; white (open) points indicate 64° data points.

direction of sliding has no systematic effect on the resistance to sliding, at least within the sensitivity of the measurements.

4. DISCUSSION

The observation that the shear stress at 'failure' scales linearly with the normal stress across the sliding plane is not surprising. Such behavior has been observed earlier for ice sliding slowly across natural Coulombic shear faults (Schulson and others, 2006b; Fortt and Schulson, 2007) at the speed and temperature applied in the present tests. The sliding resistance thus obeys Coulomb's failure criterion

$$\sigma_{nt} = \sigma_0 + \mu\sigma_{nn}, \tag{3}$$

where, again, σ_{nt} is the shear stress on the sliding plane, μ the kinetic coefficient of friction and σ_{nn} the normal stress across the sliding plane; σ_0 is the cohesive strength. Barring the variations with displacement noted above and averaging over the results over all displacement, $\sigma_0 = 0.02 \pm 0.02$ MPa and $\mu = 0.20 \pm 0.03$, in agreement with values derived by Kennedy and others (2000) and by Montagnat and Schulson (2003) from double-shear experiments on the same kind of ice under similar experimental conditions.

A modification of Coulomb's criterion, which includes the other normal stress, may be written as

$$\sigma_{nt} = \sigma_0 + \mu\sigma_{nn} + \kappa\sigma_{tt}, \tag{4}$$

where κ denotes the sensitivity of the sliding resistance to the normal stress parallel to the sliding direction. The observation that there is essentially no effect of this stress component, namely that $d\sigma_{nt}/d\sigma_{tt} \sim 0$, suggests that this component is not a significant factor in sliding resistance under the conditions tested here. Therefore, under the present conditions $\kappa \approx 0$.

We do not know whether $\kappa \approx 0$ under other conditions. Friction of ice is a complicated property and depends upon both sliding speed and temperature. For instance, at higher sliding velocities ($V_S > 10^{-5}$ m s^{-1} at –10°C), ice exhibits velocity weakening, evident from the fact that the kinetic coefficient of friction decreases with increasing sliding speed (Kennedy and others, 2000; Maeno and others, 2003; Fortt and Schulson, 2007). Under such conditions, localized melting appears to play an important role (Kennedy and others, 2000; Hatton and others, 2009). Our experiments were performed within this velocity-weakening regime, and so melting could perhaps account for the apparent absence of an effect of σ_{tt}. At lower sliding velocities ($V_S < 10^{-5}$ m s^{-1}), the character of sliding changes: sliding resistance exhibits velocity strengthening (Fortt and Schulson, 2007), and the governing mechanism appears to be localized creep (Kennedy and others, 2000; Fortt and Schulson, 2007). Whether an effect of σ_{tt} might be detectable within the velocity-strengthening regime remains to be seen. There is also a question of whether the sliding behavior of sea ice or of extraterrestrial ice differs from that of freshwater ice, owing to the presence within sea ice (Weeks, 2010) of additional

https://doi.org/10.3189/002214311798043771 Published online by Cambridge University Press

phases (brine, air and, at lower temperatures, precipitated salts) and (possibly) within extraterrestrial ice of hydrated salts (McCord and others, 1998). Although we cannot offer a firm answer, our sense is that the similarity here may be greater than the difference, at least in the case of sea ice where the friction coefficient of the two materials within the velocity-weakening regime is almost identical (Kennedy and others, 2000). Finally, one might wonder whether spatial scale is a factor. Again, we cannot offer a firm statement. However, given that the brittle compressive failure envelope of the arctic sea-ice cover has the same slope as one generated in the laboratory from specimens harvested from the winter sea-ice cover (Weiss and others, 2007), and given that the slope of the brittle compressive failure envelope is governed by the friction coefficient (Schulson and others, 2006b), our sense is that the character of sliding within the sea-ice cover is probably similar to that within test specimens. Clearly, more work is needed before the generality of the present finding can be assessed.

5. CONCLUSION

At this juncture, therefore, we conclude that there is no evidence that the resistance to sliding of warm (–10°C), freshwater ice upon itself at a relatively low speed (8×10^{-4} m s^{-1}) under low normal stresses (<1.2 MPa) is affected by the component of normal stress parallel to the direction of sliding.

ACKNOWLEDGEMENTS

We acknowledge helpful comments from F.E. Kennedy. This work was supported by NASA Outer Planets Research award No. NNX09AU27G and by US National Science Foundation grant No. ARC-0520375.

REFERENCES

Fortt, A.L. and E.M. Schulson. 2007. The resistance to sliding along Coulombic shear faults in ice. *Acta Mater.,* **55**(7), 2253–2264.

Hatton, D.C., P.R. Sammonds and D.L. Feltham. 2009. Ice internal friction: standard theoretical perspectives on friction codified, adapted for the unusual rheology of ice, and unified. *Philos. Mag.,* **89**(31), 2771–2799.

Kattenhorn, S. 2004. Strike–slip fault evolution on Europa: evidence from tailcrack geometries. *Icarus,* **172**(2), 582–602.

Kennedy, F.E., E.M. Schulson and D.E. Jones. 2000. The friction of ice on ice at low sliding velocities. *Philos. Mag. A,* **80**(5), 1093–1110.

McCord, T.B. *and 12 others*. 1998. Salts on Europa's surface detected by Galileo's near infrared mapping spectrometer. *Science,* **280**(5367), 1242–1245.

Maeno, N., M. Arakawa, A. Yasutome, N. Mizukami and S. Kanazawa. 2003. Ice–ice friction measurements, and water lubrication and adhesion-shear mechanisms. *Can. J. Phys.,* **81**(1–2), 241–249.

Michel, B. and R.O. Ramseier. 1971. Classification of river and lake ice. *Can. Geotech. J.,* **8**(1), 36–45.

Montagnat, M. and E.M. Schulson. 2003. On friction and surface cracking during sliding of ice on ice. *J. Glaciol.,* **49**(166), 391–396.

Moritz, R.E. and H.L. Stern. 2001. Relationships between geostrophic winds, ice strain rates and the piecewise rigid motions of pack ice. *In* Dempsey, J.P. and H.H. Shen, *eds. Proceedings of IUTAM Symposium on Scaling Laws in Ice Mechanics and Ice Dynamics, 13–16 June 2000, Fairbanks, AK, USA*. Dordrecht, etc., Kluwer Academic, 335–348.

Nimmo, F., J.R. Spencer, R.T. Pappalardo and M.E. Mullen. 2007. Shear heating as the origin of the plumes and heat flux on Enceladus. *Nature,* **447**(7142), 289–291.

Schreyer, H.L., D.L. Sulsky, L.B. Munday, M.D. Coon and R. Kwok. 2006. Elastic-decohesive constitutive model for sea ice. *J. Geophys. Res.,* **111**(C11), C11S26. (10.1029/2005JC003334.)

Schulson, E.M. 2004. Compressive shear faults within Arctic sea ice: fracture on scales large and small. *J. Geophys. Res.,* **109**(C7), C07016. (10.1029/2003JC002108.)

Schulson, E.M., A.L. Fortt, D. Iliescu and C.E. Renshaw. 2006a. Failure envelope of first-year Arctic sea ice: the role of friction in compressive fracture. *J. Geophys. Res.,* **111**(C11), C11S25. (10.1029/2005JC003235.)

Schulson, E.M., A.L. Fortt, D. Iliescu and C.E. Renshaw. 2006b. On the role of frictional sliding in the compressive fracture of ice and granite: terminal vs. post-terminal failure. *Acta Mater.,* **54**(15), 3923–3932.

Smith-Konter, B. and R.T. Pappalardo. 2008. Tidally driven stress accumulation and shear failure of Enceladus's tiger stripes. *Icarus,* **198**(2), 435–451.

Tufts, B.R., R. Greenberg, G. Hoppa and P. Geissler. 1999. Astypalaea Linea: a large-scale strike–slip fault on Europa. *Icarus,* **141**(1), 53–64.

Weeks, W.F. 2010. *On sea ice*. Fairbanks, AK, University of Alaska Press.

Weiss, J., E.M. Schulson and H.L. Stern. 2007. Sea ice rheology from in-situ, satellite and laboratory observations: fracture and friction. *Earth Planet. Sci. Lett.,* **255**(1–2), 1–8.

MS received 3 May 2011 and accepted in revised form 19 August 2011